

Wave climate variability in the North-East Atlantic Ocean over the last six decades

Guillaume Dodet^{a,b,*}, Xavier Bertin^{a,*}, Rui Taborda^b

^aEstuaries and Coastal Zones Division, National Laboratory of Civil Engineering, Avenida do Brasil 101, 1700-066 Lisbon, Portugal

^bFaculty of Science of the University of Lisbon, LATTEX, IDL, Bloc C-6, 2^o Floor, Campo Grande, 1749-016 Lisbon, Portugal

ARTICLE INFO

Article history:

Received 13 July 2009

Received in revised form 12 October 2009

Accepted 28 October 2009

Available online 1 November 2009

Keywords:

Wave climate variability

NAO index

North-East Atlantic Ocean

Long-term trends

ABSTRACT

Ocean surface gravity waves play a major role in many engineering and environmental problems, both in the open ocean and in coastal zones. Therefore, it is essential to improve our knowledge on spatial and temporal variability of wave climate. This study aims at investigating this variability in the North-East Atlantic Ocean (25°W–0°W and 30°N–60°N), using a 57-year hindcast (1953–2009) obtained with a spectral wave model forced with reanalysis wind fields. The hindcast analysis reveals firstly strong seasonal fluctuations of wave climate, with winters characterized by large and long-period waves of mean direction spreading from south-west to north-west, and summers characterized by smaller and shorter-period waves originating from norther directions. From northern (55°N) to southern (35°N) latitudes, the significant wave height (Hs) decreases by roughly 40%, the mean wave direction (Mwd) rotates clockwise by about 25% while the peak period (Tp) only grows by 5%. These three parameters also exhibit a strong inter-annual variability, particularly when winter-means (from 1st of December to 1st of April) are considered. Linear trend analysis over the studied period shows spatially variable long-term trends, with a significant increase of Hs (up to 0.02 m yr⁻¹) and a counterclockwise shift of Mwd (up to -0.1° yr⁻¹) at northern latitude, contrasting with a fairly constant trend for Hs and a clockwise shift of Mwd (up to +0.15° yr⁻¹) at southern latitudes. Long-term trends of Tp are less significant, with still a slight increase in the north-eastern part of the study area (up to +0.01 s yr⁻¹). Eventually, a comparison between the inter-annual variability of the winter-means of the three selected wave parameters and the North Atlantic Oscillation (NAO) reveals: (1) a strong positive correlation between Hs and the NAO index at northern latitudes (correlation coefficient up to $R = 0.91$) and a significant negative correlation at southern latitudes (up to $R = -0.6$); (2) no significant correlation for Mwd north of 40°N and a clear positive correlation southward of 40°N (up to $R = 0.8$) and (3) a northward increasing correlation for Tp (up to $R = 0.8$). Long-term trends for Hs, Mwd and Tp are finally explained by a significant increase in the NAO index over the studied period.

© 2009 Elsevier Ltd. All rights reserved.

1. Introduction

Ocean surface gravity waves constitute one of the most tangible evidence of the important exchange of energy and momentum at the ocean–atmosphere interface. As they travel across the ocean basins, waves transport the energy they accumulated during storm events and dissipate it through many processes, whose comprehension is of the prime importance for off-shore and coastal engineering and environmental issues. For instance, waves generate a Stokes drift that can significantly contribute to the dispersion of pollutants (e.g. Arduin et al., 2004). When they propagate over the continental shelves, the interaction between orbital motions and the bottom creates a sorting of sediment grain size (Carter, 1988; Black and Oldman, 1999). In nearshore regions, wave deformations induce gradients of radiation stresses (Longuet-Higgins and Stewart,

1964), which result in longshore currents, rip-currents and undertows. Finally, storm waves can damage or destroy coastal and off-shore structures and ships. Since these processes are controlled mainly by wave height/energy, direction and period/wavelength, a good knowledge on the variability of these parameters is necessary for many coastal and ocean engineering studies. Indeed, a common procedure in engineering studies is to define statistical parameters (e.g. decennial wave height) based on wave records available on time-periods often too short to represent possible pluri-decadal trends. Furthermore, the recent concerns raised by the investigation of several climate change scenarios, suggesting shifts and frequency increase of storm tracks (IPCC, 2007), make particularly relevant the need of a good assessment of long-term variability of wave climate.

During the last four decades, several studies have been undertaken to analyze wave climate change in the North Atlantic Ocean. Walden et al. (1970) examined the mean values of visually estimated wave heights from nine Ocean Weather Stations in the North Atlantic from 1950 to 1967 and revealed a high variability in wave statistics from year to year. Later, based on shipborne wave recorder data,

* Corresponding authors. Tel.: +351 218443969 (G. Dodet), +351 218443758 (X. Bertin); fax: +351 218443016.

E-mail addresses: gdodet@lnec.pt (G. Dodet), xbertin@lnec.pt (X. Bertin).

Bacon and Carter (1991) showed an increase in significant wave height (Hs) of 2.4 cm yr^{-1} for the period 1962–1986. In 1995, the Waves and Storms in the North Atlantic (WASA) project was setup to verify the hypothesis of a worsening storm and wave climate in the North-East Atlantic and concluded that the wave climate has roughened in the last decades but seemed yet to be comparable with at the beginning of this century (WASA Group, 1998). Using a 40-year wave hindcast, Wang and Swail (2001) detected an upward trend in seasonal extremes of Hs (from 1958 to 1997) with higher rates in winter in the region north-west off Ireland. However, based on a 20-year time-series of wave buoy data in the Bay of Biscay, Dupuis et al. (2006) found no particular tendency for Hs over the period 1980–1998. Kushnir et al. (1997), by combining a 10-year numerical wave hindcast and an empirical extrapolation backward in time, even suggested a decrease in wave height south of 40°N during the period 1962–1986. Therefore, it can be inferred from these last results that the wave height increase of Bacon and Carter and others may only be valid locally or at short-term scales.

In the early 1990s, a link to the North Atlantic Oscillation (NAO) was suggested by Bacon and Carter (1993) who noticed a relationship between visual estimates and instrumental records of wave heights and the atmospheric pressure gradient measured between the Iceland low and the Azores high, represented by the NAO index (Hurrell, 1995). However, these results were obtained from a few isolated weather ships and buoys located northward of 50°N , and were not sufficient to describe the spatial distribution of the wave climate. More recently, several studies used either satellite altimetry or numerical models to investigate the wave climate in the North Atlantic Ocean. Thus, Woolf et al. (2002) analyzed data sets from the ERS-1, ERS-2 and TOPEX satellites and showed decreasing correlations between Hs and the NAO index from northern to southern latitudes over the period 1991–2000. Bauer (2001) analyzed a high-resolution wave hindcast from 1981 to 1993 using the WAM model (WAMDI, 1988) and obtained low correlations between the monthly values of the NAO index and Hs, but high correlations when using winter-mean values only. Bauer (2001) also found higher correlations at northern latitudes. Dupuis et al. (2006) locally corroborated this spatial distribution, finding no correlation between Hs and NAO index in the Bay of Biscay (43°). However, they found a weak positive correlation ($R = 0.38$) between the NAO index and the annual-mean 1/3 highest wave periods. This result suggests that comparisons between other wave parameters and the NAO index could be relevant.

This paper aims at re-examining the conclusions of the above-mentioned studies by analyzing space and time wave climate variability in the North-East Atlantic (hereafter referred to as NEA) with a 57-year numerical wave hindcast (from 1953 to 2009). In addition to this unpublished time scale, the originality of this study stems from the extension of the analysis to the mean wave direction (Mwd) and the peak period (Tp), which are also relevant for numerous engineering and environmental applications. The following section (Section 2) describes the settings and the validation of the regional model used to perform the 57-year hindcast. Section 3 analyses model results and describes the spatial and temporal wave climate variability in the NEA. Section 4 investigates the correlations between the NAO index and the selected wave parameters (Hs, Mwd, Tp). Finally the findings of previous sections are summarized and discussed in the last section (Section 5).

2. The North-East Atlantic Ocean wave model

2.1. 1-Model description

Consistent studies on space and time variability of the wave climate have long been restricted by both the spatial limitation of buoy

data (sparse and concentrated in coastal areas) and the temporal limitation of satellite altimeter data (only available since the late 1980s). To counteract these limitations, spectral wave models have been developed during the two last decades and have now reached a level of accuracy that enables reproducing Hs and Tp with errors of the order of 20% (e.g. Bidlot et al., 2007b; Rasclé et al., 2008). In this study, the wave climate in the NEA Ocean was hindcasted with the version 3.14 of the third-generation spectral wave model WAVEWATCH III™ (henceforth denoted as WW3) (Tolman, 2009). The parametrization is similar to the one used by Ardhuin et al. (2009a), with further modifications for the wind input (S_{in}) and dissipation (S_{ds}) source terms. Namely, the parametrization of S_{in} is taken from Janssen (1991) as modified by Bidlot et al. (2007a), with some modifications for the high frequency part of the spectrum (Filipot et al., 2008). The representation of white-capping dissipation is based on recent observations of wave breaking statistics (Banner et al., 2000), and swell dissipation (Ardhuin et al., 2009a). This parametrization is fully described and validated in Ardhuin et al. (2009b).

The model spatial grid covers the North Atlantic Ocean, from 80.0°W to 0.0°W in longitude and 0.0°N to 70.0°N in latitude (Fig. 1), with a 0.5° resolution. In order to satisfy the associated CFL condition, the spatial propagation time-step was set to 15 min. The bathymetry originates from the 2-min global seafloor topography derived from satellite altimetry and ship depth soundings by Smith and Sandwell (1997). The spectral grid uses 24 regularly spaced directions and extends from 0.041 Hz to 0.41 Hz with 20 exponentially spaced frequencies.

The model was forced with 6-h wind fields from the NCEP/NCAR Reanalysis project (Kalnay et al., 1996), available from 1953 to present, on a 1.875° (longitude) by $\sim 1.905^\circ$ (latitude) Gaussian grid, where longitudes are equally spaced but latitudes are unequally spaced according to Gaussian quadrature. Wind fields were then interpolated on a regular 0.5° grid to force the model. Wave interactions with currents were not considered in this study, assuming they are negligible at the scale of the North Atlantic Ocean. Ice coverage was neither taken into account since the required data was not available over the whole studied period. Moreover, the assumption was made that ice coverage has only a weak impact on wave climate in the area considered in this study. This assumption is corroborated by Tolman (2002), who showed only minor improvements for wave predictions in this specific area when considering ice coverage.

A 57-year simulation was performed from 1953 to 2009 and provided 6-h time-series of Hs, Mwd and Tp over a box extending from 25.0°W to 0°W and from 30.0°N to 60.0°N , which corresponds to the NEA Ocean mentioned above. In order to deal with the very large subsequent computational cost, the Message Passing Interface (MPI) version of WW3 was used on a 268 processors Fujitsu-Siemens PC-cluster. The whole simulation was split into six 10-year runs, each of them running on 20 processors within 30 h. In order to quantify seasonal variability of wave climate, winter – (between 1st December and 1st April) and summer – (between 1st June and 1st October) means were computed for each parameters. Since the most energetic wave conditions are of key importance for navigation, offshore and coastal engineering applications, the yearly mean of Hs values higher than the annual Hs 90th percentile (threshold value below which 90% of Hs values are found) was computed and is referred to as H_{s90} . A three steps procedure was used to process Mwd in order to avoid problems related to this variable that goes over a circle: (1) Mwd was decomposed into zonal and meridional components; (2) means of each component were computed and (3) mean Mwd was reconstructed using an Arctangent 2 function.

Long-term variability of wave climate and potential correlations with the NAO were then investigated by analyzing time-series of these variables.

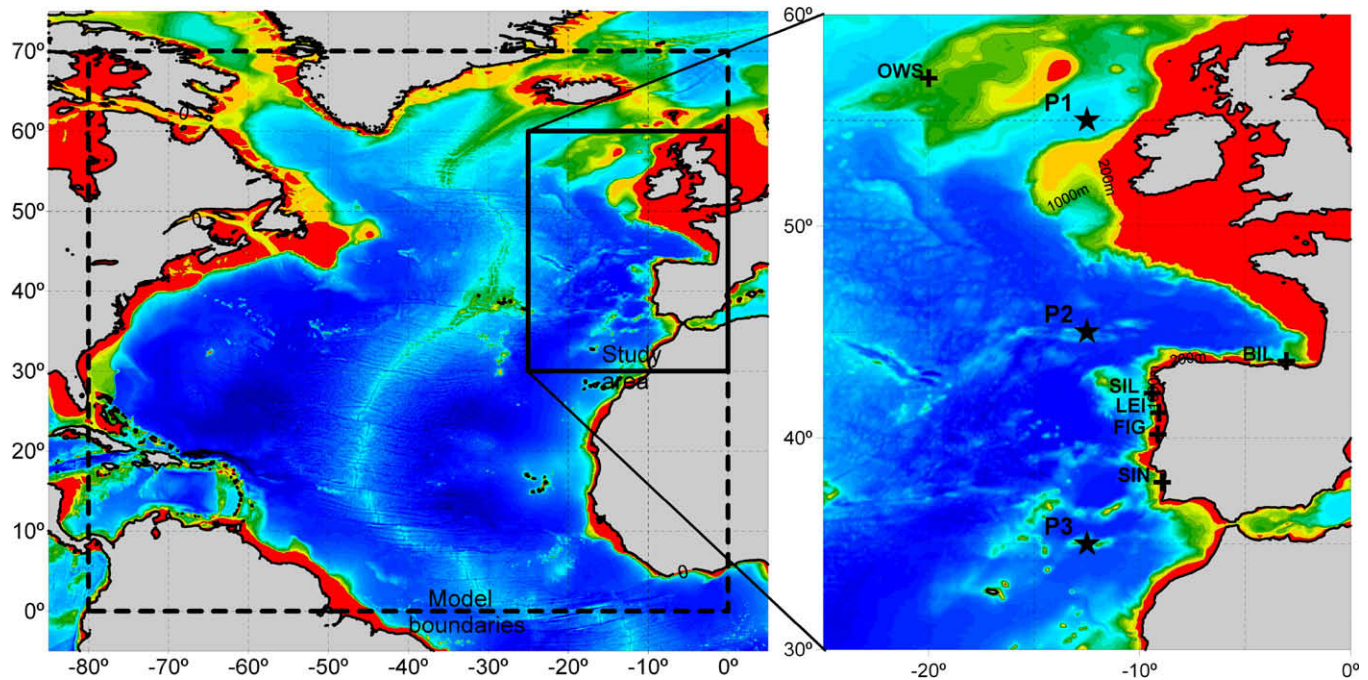


Fig. 1. Bathymetric map of the North Atlantic Ocean showing the extension of the modelled area (left) and study area referred to as North-East Atlantic Ocean (right). Location of wave buoys Bilbao-Vizcaya (BIL), Cabo Silleiro (SIL), Leixões (LEI), Figueira da Foz (FIG), Sines (SIN) and Ocean Weather Station “Juliett” (OWS) and three selected model output locations (P1, P2 and P3).

2.2. 2-Model validation

The model was validated against buoy data over time-period and locations (crosses on Fig. 1) covering, as much as possible, the time and space extensions of the study: three buoys off the Portuguese coast – Sines (SIN), Leixões (LEI) and Figueira da Foz (FIG) – and two buoys off the Spanish coast – Cabo Silleiro (SIL) and Bilbao-Vizcaya (BIL). An additional comparison was realized with data from the Ocean Weather Station (OWS) “Juliett” (20.0°W; 52.5°N) to cover the period 1952–1975. Model outputs used for validation were taken at grid nodes and thus do not always match exactly buoy locations. However, this problem was only relevant at the FIG station, where the output node was selected seawards of the exact location. Further details on the locations and time-periods for buoys and OWS are given in Table 1.

Before being compared against model results, the data of each buoy was processed following a common methodology: (1) Mwd was corrected to take into account the magnetic declination occurring at the specific location and time-period; (2) Hs, Mwd and Tp were averaged using (2a) 6-h and (2b) 1-month sliding windows; and (3) these values were finally interpolated on (3a) 6-h and (3b) 1-month regularly spaced time vectors. For consistent comparisons between model and data, steps (2b) and (3b) were also applied to model outputs. The 6-h time-window was chosen to consistently compare data against 6-h model outputs, corresponding to the temporal resolution of wind forcing. The 1-month time-window was

chosen to evaluate model precision when investigating long-term trends and correlation with the NAO index. Comparisons between 6-h averaged data and model outputs are shown in Figs. 2–4 for OWS “Juliett”, and Figueira da Foz (FIG) and Bilbao (BIL) buoys, respectively. In these figures as well as in the rest of this paper, values of Mwd correspond to the incoming wave direction relative to North and increase clockwise. Figs. 2–4 illustrate model capacity to fairly reproduce Hs, Mwd and Tp over a 6 month period. In larger details, it can be noted at the location of the Bilbao buoy that the model fails to reproduce short term (i.e. less than 1 day) shift in Mwd from NW to NE and decrease in Tp. The occurrence of these short-term shifts in Mwd and Tp while Hs remains constant is due to the superimposition of two wave regimes: a first one corresponding to long-period swells coming from the NW and a second one associated to local NE winds. Better predictions of these two parameters were obtained by nesting locally a higher resolution grid fed by higher resolution wind fields, but are not presented here as they fall outside the scope of this study.

Fig. 5 corresponds to scatter diagrams of measured versus modelled Hs for the entire dataset and shows an overall good agreement between measured and predicted Hs. It can be seen qualitatively that the model reproduces both weak and energetic waves with a similar accuracy, although a linear regression reveals a negative bias of the order of 0.20 m. A comparison between Fig. 5A and B shows how predictions are improved by averaging the dataset over 1 month (Fig. 5B) instead of 6 h (Fig. 5A).

Table 1
Characteristics of wave data used for the model validation.

Station name and abbreviation	Location	Depth (m)	Period	Number of samples	Data coverage (%)	Type of instrument
OWS Juliett (OWS)	20.00°W; 57.00°N	2500	1954/11–1975/09	4368	6.6	Shipborne wave recorder
Bilbao-Vizcaya (BIL)	3.04°W; 43.63°N	600	1990/11–2009/04	72,148	66.4	Seawatch (oceanor)
Cabo Silleiro (SIL)	9.40°W; 42.12°N	323	2003/06–2009/04	48,623	86.1	Seawatch (oceanor)
Leixões (LEI)	9.09°W; 41.20°N	83	1993/08–1995/01	2836	63.3	Wavec (datawell)
Figueira da Foz (FIG)	9.15°W; 40.19°N	83	1993/01–1995/12	5327	57.3	Wavec (datawell)
Sines (SIN)	8.93°W; 37.92°N	97	1993/01–1995/12	5356	60.2	Wavec (datawell)

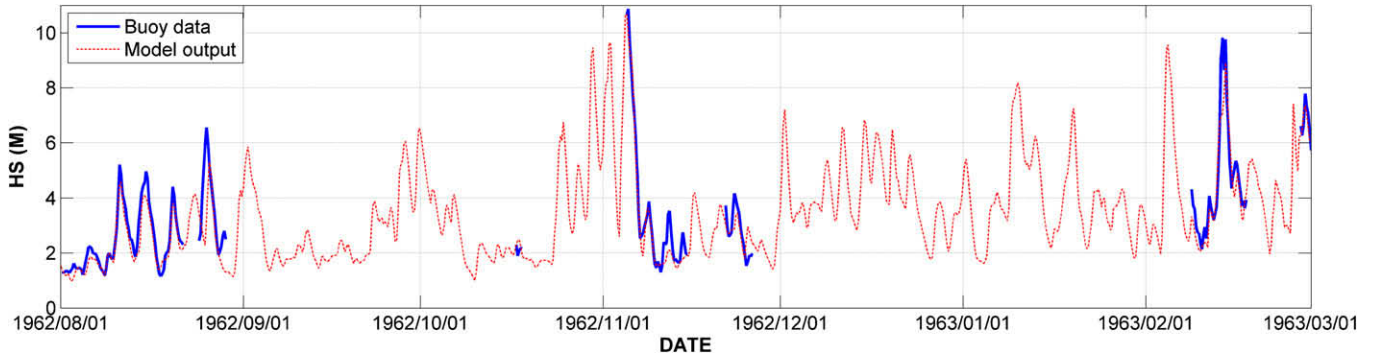


Fig. 2. Comparison between 6-h modelled and measured Hs at Ocean Weather Station (OWS) “Juliett” between August 1962 and March 1963.

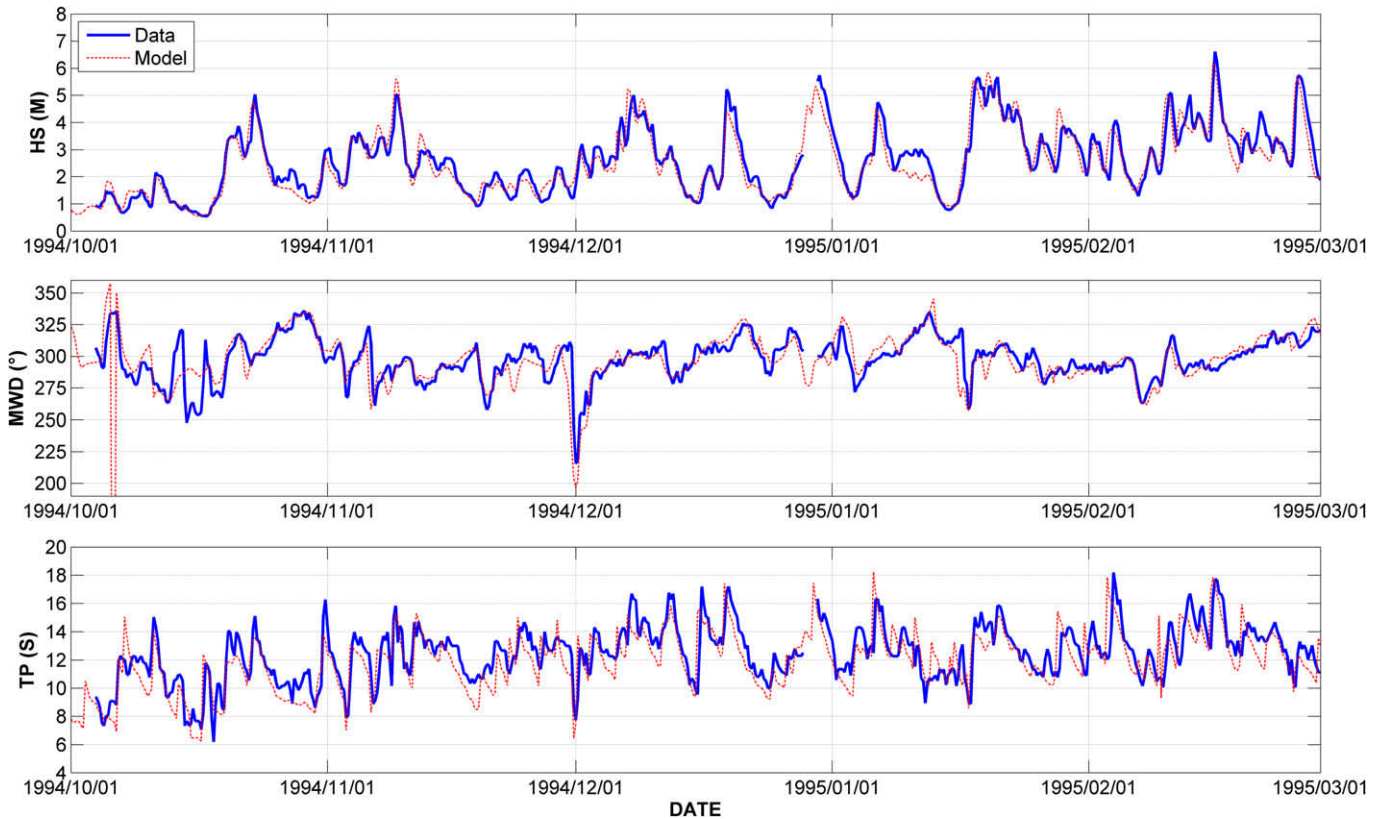


Fig. 3. Comparison between 6-h modelled and measured Hs (top), Mwd (middle) and Tp (bottom) at Figueira da Foz from October 1994 to April 1995.

Bias and Root Mean Square Error (RMSE) were computed for every parameter (Table 2). For Hs and Tp, the RMSE was normalized by the mean of the observed values (NRMSE). In order to quantify the accuracy of model predictions for winter-means (4 months), this statistical analysis was also applied to monthly averaged data. 4-monthly average were also considered and resulted in smaller errors tending towards the bias. However, these values are not presented here due to the lack of 4 month periods without any gaps in the buoy datasets. It can thus be assumed that errors for 4-month means predictions are significantly smaller than those derived from the 1-month average analysis. Comparisons between model and data revealed RMSE of the order of 0.50 m, 20° and 2 s with 6-h average and 0.15 m, 5° and 1 s with monthly average, for Hs, Mwd and Tp, respectively (Table 2). A systematical negative bias in Hs of the order of 0.10 m to 0.30 m can be observed at every station. Slightly better predictions for Hs were obtained by tuning parameters for the source terms, but this parameterization resulted in less accurate predictions for Mwd and Tp.

3. Temporal and spatial wave climate variability

In order to describe the temporal and spatial variability of wave climate in the NEA, 57-year time-series of Hs, Mwd and Tp were plotted at the longitude 12.5°W for three different latitudes: 55°N, 45°N and 35°N, hereafter referred to as P1, P2 and P3, respectively (see Fig. 1). These three locations present depths larger than 1000 m and thus provide deep-water wave characteristics.

3.1. Wave height

The 3-monthly averaged Hs (Fig. 6) display a large seasonal variability, with an amplitude that decreases from North to South (P1–P3). Thus during summer months, Hs are of the order of 2.0 m, 1.6 m and 1.4 m from P1 to P3 while during winter months, Hs are of the order of 4.5 m, 3.5 m and 2.5 m, respectively. A similar tendency as for Hs is observed for Hs₉₀, with average values of

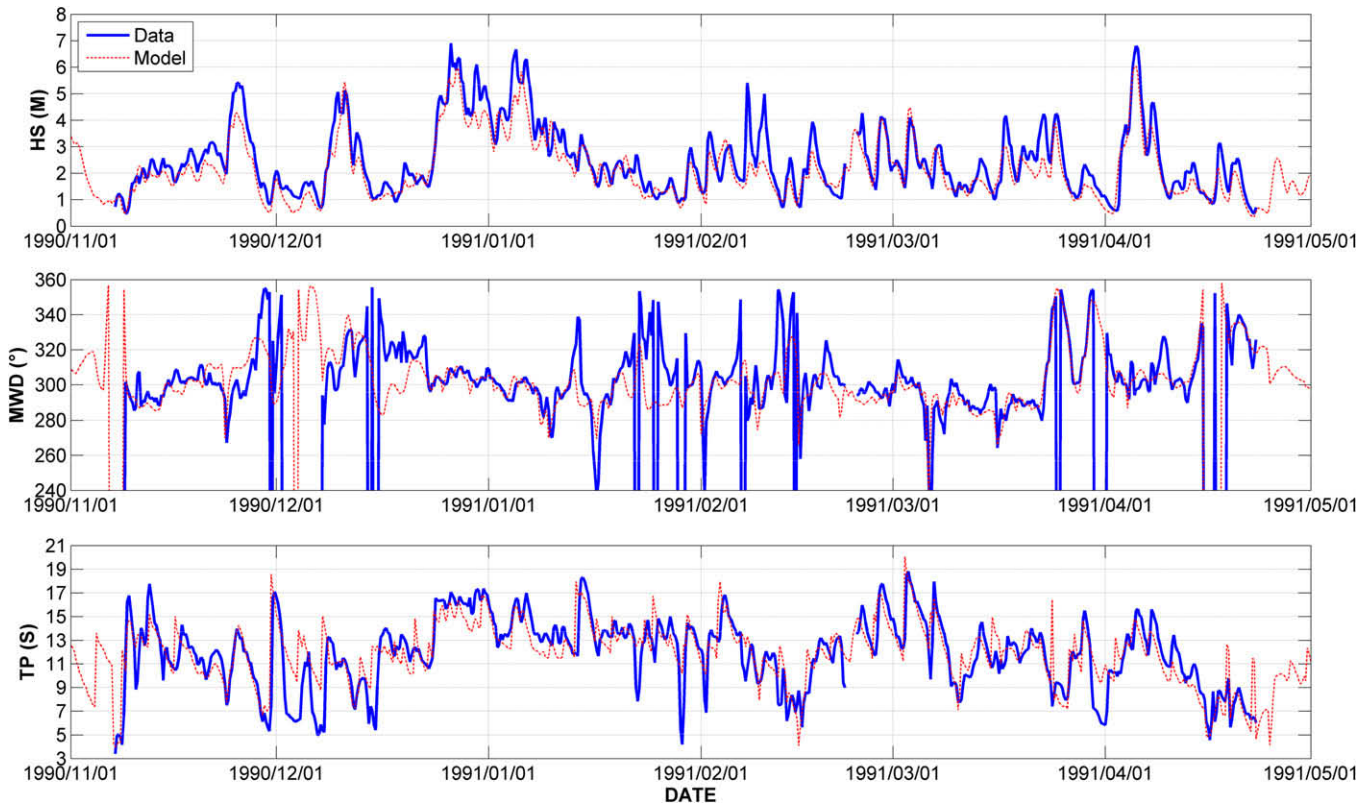


Fig. 4. Comparison between 6-h modelled and measured Hs (top), Mwd (middle) and Tp (bottom) at Bilbao-Vizcaya from November 1990 to May 1991.

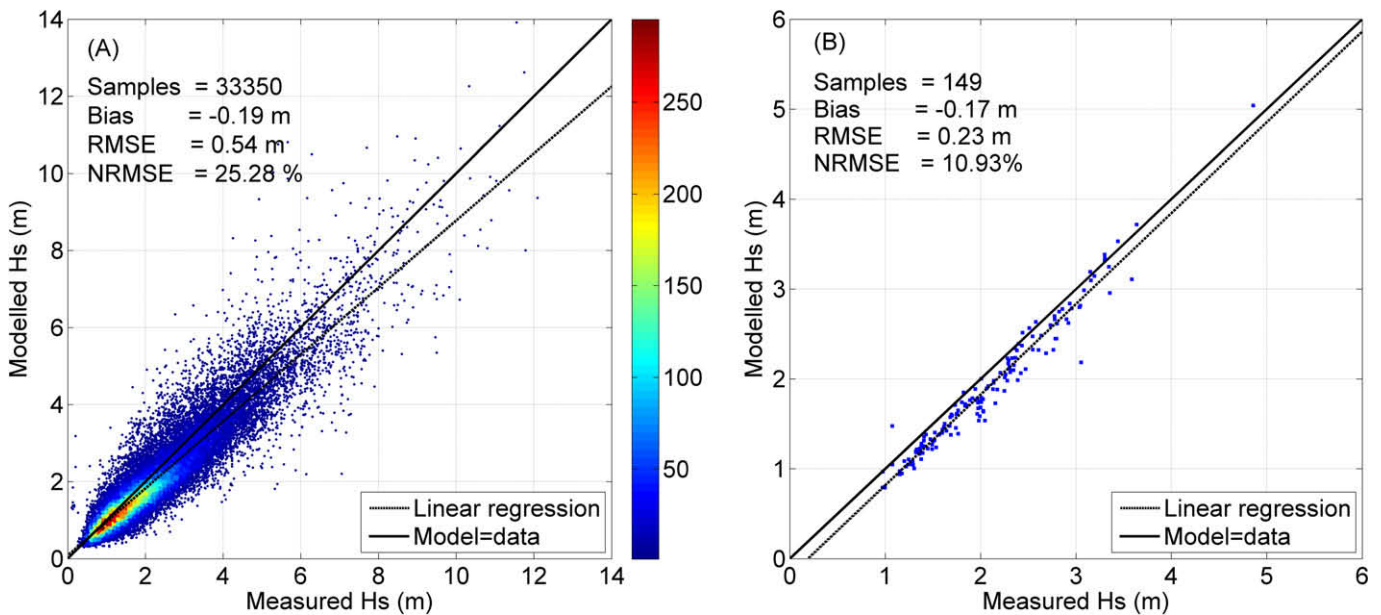


Fig. 5. Scatter diagrams of 6-h (A) and 1-month (B) modelled Hs versus measured Hs for the entire data set. The color bar on the left panel corresponds to sample density and is arbitrarily expressed in number of point per $0.10 \text{ m} \times 0.10 \text{ m}$ squares. The solid line corresponds to $y = x$, the dashed line to a linear regression and the difference between both lines illustrates the slight negative bias of modelled Hs. (For interpretation of color mentioned in this figure the reader is referred to the web version of the article.)

7.5 m for P1, 6.0 m for P2 and 4.0 m for P3. Moreover, a larger variability of Hs_{90} is observed from P1 to P3, as illustrated by standard deviations (σ) of 0.66 m, 0.50 m and 0.34 m, respectively. The summer-means of Hs display a much weaker variability, of the order of 0.15 m (Table 3) compared to Hs_{90} and Hs winter-means. Winter-mean values for Hs were not plotted on Fig. 6 for clarity reason, but comparisons between winter-mean Hs and Hs_{90}

showed that over 70% of Hs_{90} occurrence take place during winter months. Long-term trends for Hs_{90} and Hs winter- and summer-means were evaluated by means of linear regressions (Table 3). Hs_{90} and Hs winter-means display a strong upward trend at P1, a weakly positive trend at P2 and no significant trend at P3. On the contrary, summer-means of Hs don't show any significant trends (Table 3). The spatial variability of Hs_{90} long-term trend was

Table 2

Statistical results of model/data comparison at each buoy location: Number of entries, Bias, Root Mean Square Error (RMSE) and Normalized (by the mean of observed values) Root Mean Square Error (NRMSE). Six-h (resp. 1-month) columns correspond to values obtained after applying a 6-h (resp. 1-month) low-pass filter to the data. “na” refers to non-available values.

Buoy	Parameter	Number of entries		Bias		RMSE		NRMSE	
		6-h	1-month	6-h	1-month	6-h	1-month	6-h	1-month
OWS	Hs	2049	0	−0.37 m	na	0.89 m	na	24.44%	na
	Mwd	na	na	na	na	na	na	na	na
	Tp	na	na	na	na	na	na	na	na
BIL	Hs	17,018	73	−0.21 m	−0.22 m	0.53 m	0.25 m	28.08%	13.24%
	Mwd	17,018	73	−6.00°	−4.81°	20.78°	7.59°	na	na
	Tp	17,018	73	0.63 s	0.63 s	1.95 s	0.89 s	18.58%	9.01%
SIL	Hs	7853	49	−0.10 m	−0.11 m	0.50 m	0.17 m	21.89%	7.09%
	Mwd	7853	49	−3.25°	−3.92°	18.81°	6.52°	na	na
	Tp	7853	49	0.66 s	0.82 s	1.86 s	0.98 s	18.84%	10.02%
FIG	Hs	2491	10	−0.14 m	−0.14 m	0.45 m	0.18 m	20.49%	7.83%
	Mwd	2491	10	0.93°	0.87°	14.98°	3.74°	na	na
	Tp	2491	10	−0.38 s	−0.45 s	1.60 s	0.52 s	14.2%	4.6%
LEI	Hs	1318	2	−0.12 m	−0.13 m	0.48 m	0.15 m	19.95%	8.49%
	Mwd	1318	2	2.73°	3.54°	15.74°	4.63°	na	na
	Tp	1318	2	−0.29 s	−0.25 s	1.51 s	0.34 s	13.54%	3.76%
SIN	Hs	2621	15	−0.26 m	−0.26 m	0.40 m	0.27 m	25.59%	18.33%
	Mwd	2621	15	0.39°	0.80°	16.36°	4.26°	na	na
	Tp	na	na	na	na	na	na	na	na

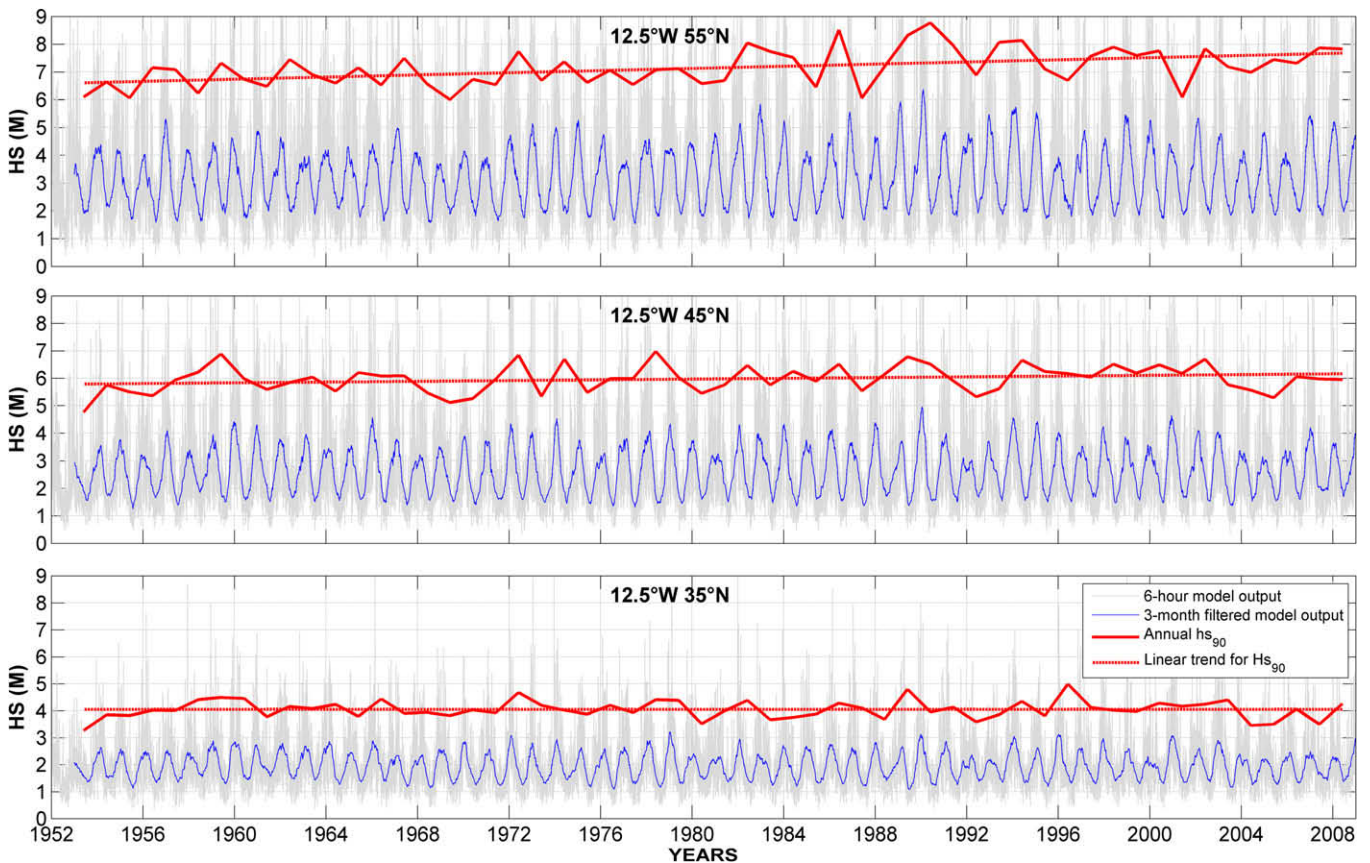


Fig. 6. Time-series of 6-h modelled Hs (grey), 3-month filtered modelled Hs (blue line), Hs90 (red solid line) and linear trend for Hs90 (red dashed line) at P1 (top), P2 (middle) and P3 (bottom) from 1953 to 2009. (For interpretation of color mentioned in this figure the reader is referred to the web version of the article.)

further investigated and is plotted on Fig. 9A. This analysis revealed an increase in Hs₉₀ at northern latitudes up to 1.2 m over the study period (0.02 m yr^{−1}), which matches the 0.022 m yr^{−1} rate described by Bacon and Carter (1991). This upward trend decreases southward until latitudes 40°N, after which no significant tendency is observed.

3.2. Wave direction

A similar analysis carried out for Mwd show that mean values of 3-monthly averaged Mwd increase from North to South (281° at P1, 309° at P2 and 326° at P3) (Fig. 7). As observed for Hs, Mwd exhibits a strong seasonal variability for the three studied locations, with

Table 3
Statistics of modelled wave parameters (H_{s90} , summer- and winter-means of H_s , Mwd and Tp) at the three selected locations (P1, P2 and P3); mean, standard deviation (std) and linear trend (values in brackets give the gain calculated over the 57-year period).

Point name	P1			P2			P3		
	Mean	Std	Linear trend	Mean	Std	Linear trend	Mean	Std	Linear trend
Coordinates	12.5°W; 55.01°N			12.5°W; 45.01°N			12.5°W; 35.01°N		
Parameter	Mean	Std	Linear trend	Mean	Std	Linear trend	Mean	Std	Linear trend
H_{s90}	7.14 m	0.66 m	0.0190 m yr ⁻¹ (1.08 m)	5.97 m	0.50 m	0.0068 m yr ⁻¹ (0.39 m)	4.05 m	0.34 m	-0.00002 m yr ⁻¹ (-0.001 m)
Winter-mean H_s	4.33 m	0.55 m	0.0118 m yr ⁻¹ (0.67 m)	3.55 m	0.37 m	0.0019 m yr ⁻¹ (0.11 m)	2.48 m	0.24 m	-0.0016 m yr ⁻¹ (-0.09 m)
Summer-mean H_s	2.13 m	0.16 m	0.0013 m yr ⁻¹ (0.07 m)	1.72 m	0.13 m	0.0016 m yr ⁻¹ (0.09 m)	1.39 m	0.10 m	-0.0004 m yr ⁻¹ (-0.02 m)
Winter-mean Mwd	260°	11.54°	-0.0257° yr ⁻¹ (-1.48°)	284°	10.57°	-0.0581° yr ⁻¹ (-3.31°)	317°	7.27°	0.0901° yr ⁻¹ (5.13°)
Summer-mean Mwd	268°	7.67°	-0.0410° yr ⁻¹ (-2.36°)	310°	8.03°	-0.0018° yr ⁻¹ (-0.10°)	336°	3.69°	0.090° yr ⁻¹ (5.13°)
Winter-mean Tp	11.1 s	0.44 s	0.0070 s yr ⁻¹ (0.40 s)	11.6 s	0.50 s	0.0051 s yr ⁻¹ (0.29 s)	11.8 s	0.43 s	0.0022 s yr ⁻¹ (0.13 s)
Summer-mean Tp	8.34 s	0.23 s	0.0039 s yr ⁻¹ (0.22 s)	8.29 s	0.20 s	0.0034 s yr ⁻¹ (0.19 s)	8.21 s	0.26 s	0.0070 s yr ⁻¹ (0.40 s)

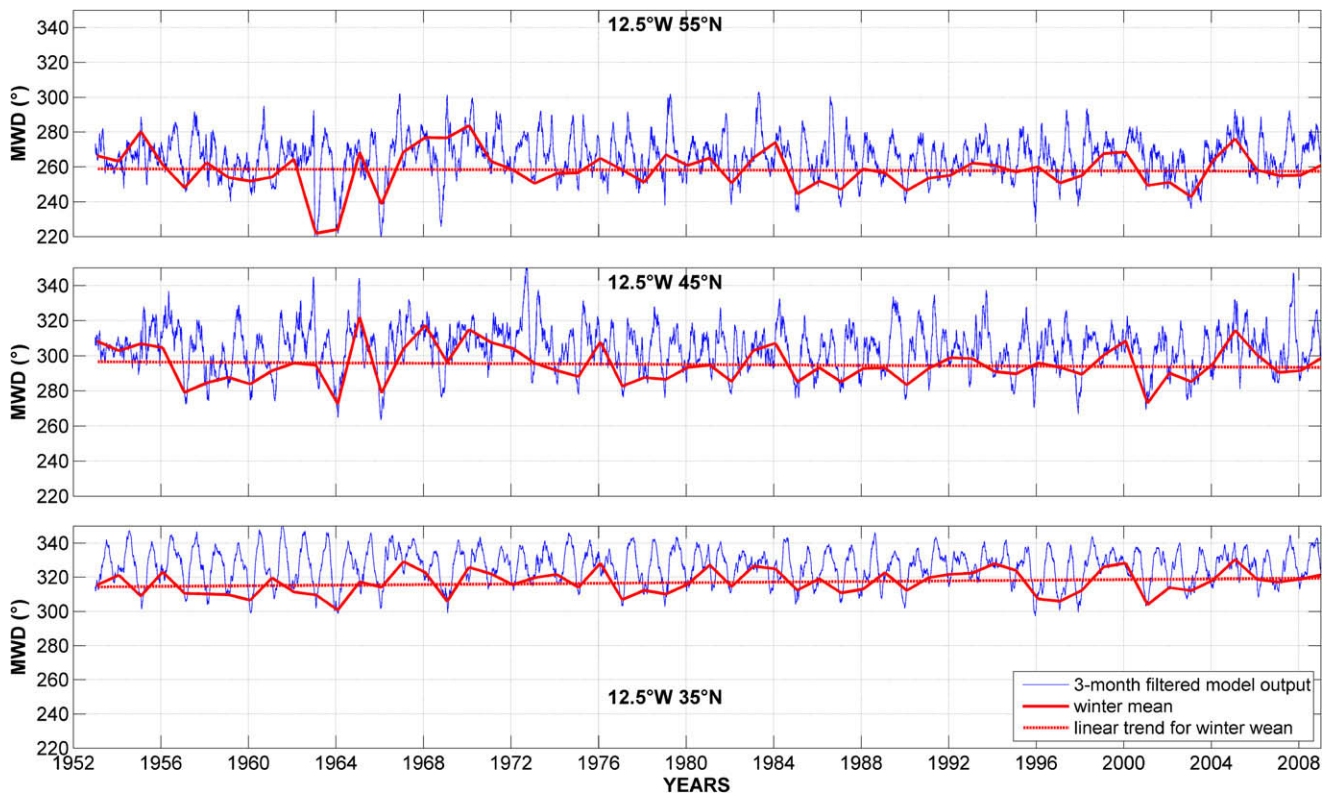


Fig. 7. Time-series of 3-month filtered modelled Mwd (blue line), winter-mean modelled Mwd (red solid line) and linear trend for winter-mean modelled Mwd (red dashed line), at P1 (top), P2 (middle) and P3 (bottom) from 1953 to 2009. Six-h modelled Mwd is not shown for clarity reason. (For interpretation of color mentioned in this figure the reader is referred to the web version of the article.)

summer directions generally 20°–80° norther than winter directions. However, Mwd at northern latitudes are characterized by a less regular seasonal signal than at southern latitudes and even opposite behaviors can be observed at P1 (e.g. summer 1968). As described above, winter season corresponds to the most energetic period of the year regarding H_s . Consequently, winter-means of Mwd provide a good indication of the direction associated to these energetic waves. Once again, larger inter-annual variabilities for winter-means of Mwd are observed from northern to southern latitudes ($\sigma = 11.5^\circ$, $\sigma = 10.6^\circ$ and $\sigma = 7.3^\circ$, for P1, P2 and P3, respectively). Comparing to winter-means, summer-means of Mwd are characterized by a 30–50% smaller variability ($\sigma = 7.7^\circ$, $\sigma = 8.0^\circ$ and $\sigma = 3.7^\circ$, for P1, P2 and P3, respectively) Long-term trends for Mwd winter-means, deduced from linear regression, revealed a counterclockwise shift at northern latitudes (Fig. 9B) reaching locally 5° ($-0.1^\circ \text{ yr}^{-1}$) whereas a clockwise shift up to 8° ($+0.15^\circ \text{ yr}^{-1}$) is observed at southern latitudes. Summer-means of

Mwd only exhibit significant long-term trends at southern latitudes, where a counterclockwise shift up to -5° ($-0.09^\circ \text{ yr}^{-1}$) is observed (Table 3).

3.3. Peak period

Fig. 8 presents time-series for Tp at the three locations P1, P2 and P3. Comparing to Mwd , a much more regular seasonality can be observed, with summers characterized by Tp of about 8–9 s and winters by Tp in the 11 s–13 s range. From North to South, a slight increase can be seen ($+0.5$ –1 s). For the three locations, a significant inter-annual variability of Tp winter-means can be observed, with minimum values in the late 1960s (10.5 s) and maximum values in the late 1980s (12.5 s). Comparatively, a 50% smaller variability is observed for summer-means of Tp (Table 3). Long-term evolution of Tp over the NEA shows a spatial variability that is in broad agreement with the H_{s90} pattern; negligible

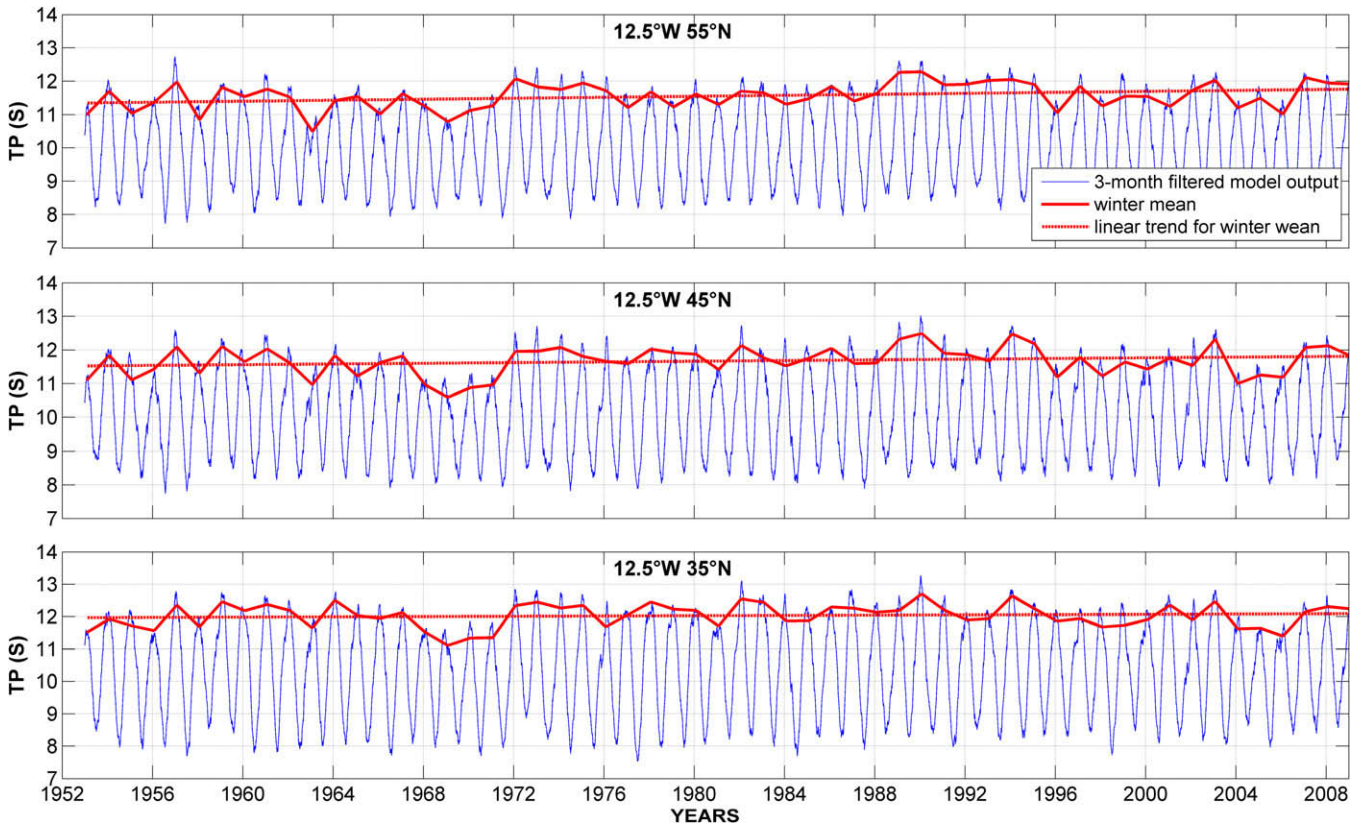


Fig. 8. Time-series of 3-month filtered modelled Tp (blue line), winter-mean modelled Tp outputs (red solid line) and linear trend for winter-mean modelled Tp (red dashed line), at P1 (top), P2 (middle) and P3 (bottom) from 1953 to 2009. Six-h model output is not shown for clarity reason. (For interpretation of color mentioned in this figure the reader is referred to the web version of the article.)

changes are depicted south-west, while an upward trend, that locally reaches +0.6 s over the studied period (Table 3), can be observed in the north-east sector (Fig. 9C). Long-term trends for summer-means of Tp are less significant and only exhibit positive trends at southern latitudes, where they reach +0.4 s over the studied period.

4. The correlation of wave climate variability with NAO

In the previous section, winter-means of Hs, Mwd and Tp were shown to display an important inter-annual variability and this variability was also shown to vary strongly in space. Comparatively, summer-means were associated to a weaker variability.

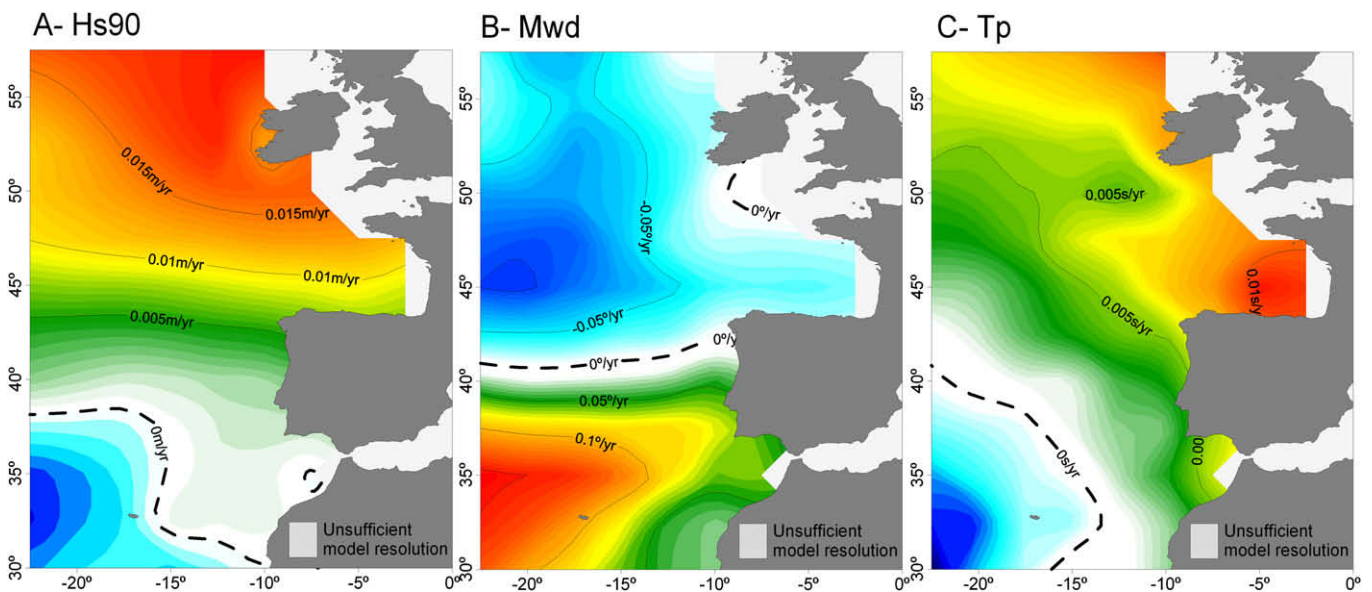


Fig. 9. Contour maps of linear trends for Hs90 (A), Mwd (B) and Tp (C) in the NEA Ocean for the period 1953–2009. Null trend is represented by the black dashed line.

Moreover, linear regressions over the whole studied period highlighted pluri-decadal trends for winter-means of these parameters and almost no significant trends for summer-means. Several authors (Bacon and Carter, 1993; Bauer, 2001; Wang and Swail, 2001; Woolf et al., 2002) have proposed that inter-annual fluctuations in Hs are controlled by NAO. Furthermore, Bauer (2001) showed that wave height was considerably more correlated with the winter NAO index than the monthly NAO index. This last finding was confirmed in an earlier stage of this study and it was thus decided to focus our analysis on winter-means only.

In order to extend this finding both in time and to other wave parameters, Pearson correlation coefficients of the winter (December–March) NAO index with Hs₉₀ and winter-means of Mwd and Tp were calculated over the NEA. The winter NAO index is based on the monthly averaged difference of normalized sea level pressure (SLP) between Lisbon, Portugal and Stykkisholmur/Reykjavik, Iceland since 1864 (Hurrell, 1995) and will be referred to as the WNAO index. Fig. 10 presents contour maps of correlation coefficients between the WNAO index and each wave parameter. Fig. 10A shows that strong correlations between Hs₉₀ and the WNAO index occur at northern latitudes (north of 55°N) with a maximum value of 0.91 at (10°W; 57.5°N). The correlation decreases then from latitude 57.5°N to latitude 45°N (with no correlation at this latitude) and then becomes negative south of 45°N, reaching −0.49 at (15°W; 30°N). The temporal variation of this correlation is illustrated in Fig. 11, where the normalized time-series of winter-mean Hs and WNAO index show a very close behavior at P1 and an opposite behavior at P3. The spatial distribution and the values obtained over this 57-year period match very well the correlation map of Woolf et al. (2002) derived from satellite altimeters from 1991 to 2000.

Regarding Mwd (Fig. 10B), it can be seen that the correlation with the WNAO index is very weak at high and middle latitudes and becomes significant southward, with a maximum value of 0.83 at (7.5°W; 35°N). Time-series of the WNAO index and Mwd are represented in Fig. 11 for P1 and P3 and illustrate the weak correlation at northern latitude ($R = 0.01$) and the higher correlation at southern latitudes ($R = 0.58$).

Finally, correlations between Tp and the WNAO index are shown in Fig. 10C. As for Hs, Tp displays a meridional distribution of the correlation coefficient with the highest values occurring at

northern latitudes and reaching a maximum of $R = 0.81$ at (12.5°W; 57.5°N). A similar spatial distribution of the correlation between the WNAO index and the mean wave period was derived from radar altimetry by Challenor et al. (2006) over the period 1993–2003. The weaker values obtained by these authors are probably due to the use of monthly-means instead of winter-means.

5. Discussion and conclusions

A first analysis of the 57-year hindcast revealed a strong seasonal variability of wave climate in the NEA. Boreal winters are characterized by large and long-period waves with mean directions spreading from south-west to north-west and summers are characterized by smaller and shorter-period waves with norther mean directions. During summer, the Azores high-pressure system dominates over the North Atlantic, whereas it weakens and moves towards the equator in winter, when the high-latitude Icelandic low-pressure center predominates (Hurrell and Dickson, 2004). This winter configuration leads to higher pressure gradients and thus stronger surface winds, resulting in more energetic wave conditions at this time of the year. Besides, the northward shift of the storm path in summer results in wave directions norther than in winter.

Winter-means of the three selected wave parameters were shown to display a significant inter-annual variability, illustrated by standard deviations of the order of 0.4 m, 10° and 0.45 s, for Hs, Mwd and Tp, respectively. Several authors (Bacon and Carter, 1993; Woolf et al., 2002; Bauer, 2001; Wang and Swail, 2001) showed a relation between the NAO and the variations of Hs within the period 1958–1997. In this study, comparisons with the WNAO index revealed a strong positive correlation between Hs₉₀ and the WNAO index at northern latitudes (up to $R = 0.91$) and a significant negative correlation at southern latitudes (up to $R = -0.6$). These spatial distribution and values computed for a 57-year period match closely the results obtained by Woolf et al. (2002) and Bauer (2001) over 10-year periods and thus strengthen the idea of a NAO control upon Hs. In addition, the extension of the analysis to other wave parameters exhibited: (1) a clear positive correlation between the WNAO index and winter-means of Mwd south of 40°N (up to $R = 0.8$) and no significant correlation north of 40°N and (2) a southward decreasing correlation for Tp winter-means with maximum values of about $R = 0.8$. To better explain these correlations, two

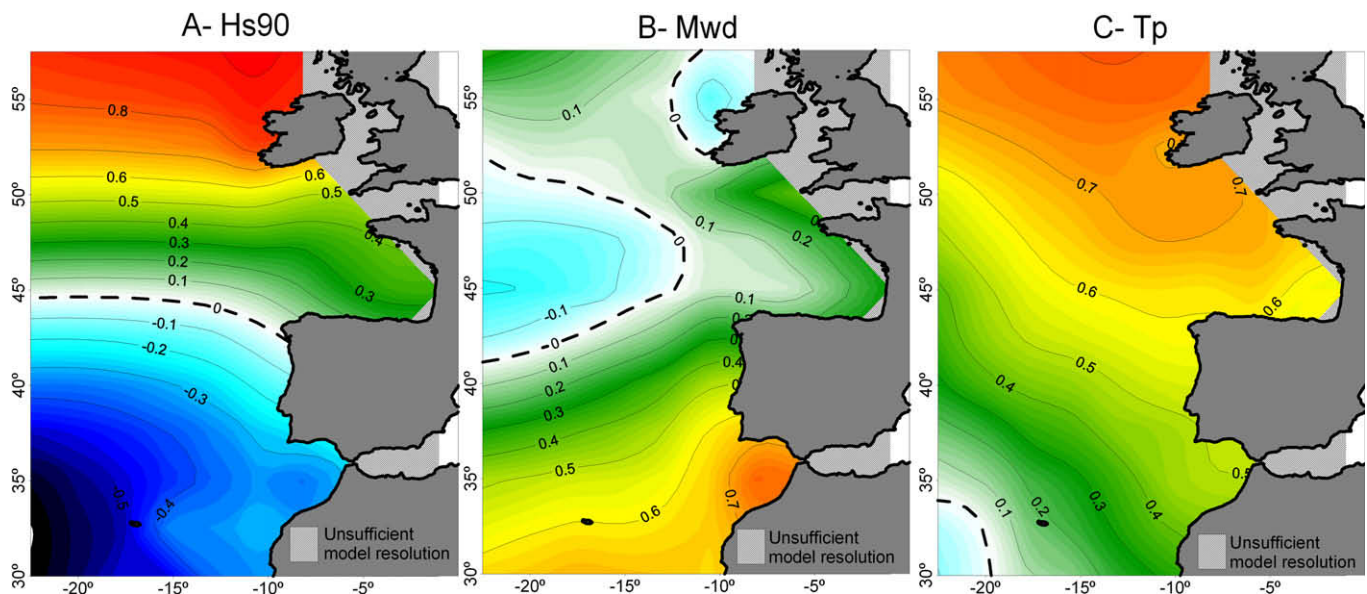


Fig. 10. Contour maps of Pearson correlation coefficients between the WNAO index and Hs₉₀ (A), Mwd winter-means (B) and Tp winter-means (C) in the NEA Ocean for the period 1953–2009. Null correlation is represented by the black dashed line.

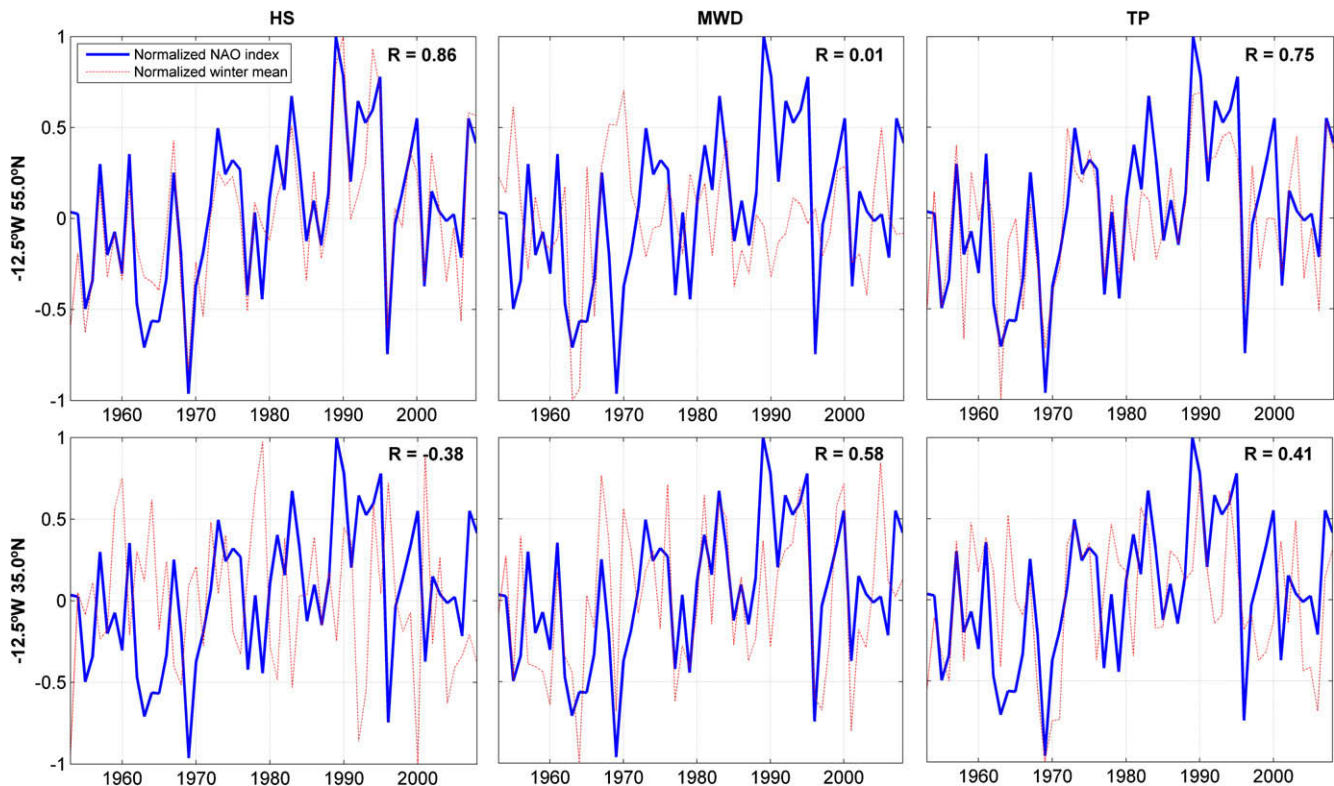


Fig. 11. Comparisons between the normalized WNAO index and winter-means of Hs, Mwd and Tp at (12.5°W; 55.0°N) (upper panel) and at (12.5°W; 35.0°N) (lower panel). The Pearson correlation coefficient is given for each subplot.

extreme NAO configurations were selected: the case “NAO–” corresponds to the winter 1969 (from 1st December 1968 to 31st March 1969) where the highest negative value was found within the WNAO index between 1953 and 2009, while the case “NAO+” refers to winter 1989 with the highest positive value in this index. Fig. 12 shows the corresponding winter-means of reanalysis sea level atmospheric pressure (SLP) and wind velocity (Kalnay et al., 1996) as well as modelled winter-mean wave spectra at P1 and P3. As explained by Hurrell (1995), NAO+ winters are associated with larger than normal SLP gradients, due to the presence of a wide and stable anticyclone centered on the Azores Islands and deep lows crossing Iceland (Fig. 12E). This configuration results in stronger than average westerly winds across the middle latitudes (Fig. 12F), inducing very large and long-period waves with a mean western direction at northern latitudes (Fig. 12G). Southern latitudes, kept off storm area, are subjected to smaller-than-normal and long-period waves coming from a very narrow north-west directional window (Fig. 12H). On the contrary, NAO– winters are associated with Icelandic low- and Azores high-pressure centers weaker-than-normal and with a more random spatial distribution, resulting in weaker middle latitude westerlies. Fig. 12C and D illustrates the wave climate associated to this negative NAO phase at P1. Namely, at northern latitudes Hs and Tp are weaker-than-average and present a huge directional spreading, while at southern latitudes Tp are medium, the directional spreading large and Hs larger-than-average. These Hs larger-than-average under NAO– situation match the negative correlation between Hs and WNAO index shown in Fig. 10 and can be explained by closer storm areas. The large directional spreading of wave energy at P1 under NAO– situation (Fig. 12C) displays a bi-modal structure due to the presence of a northern component, which does not appear under NAO+ condition (Fig. 12G). This northern component in the wave spectrum can be related to the presence of northern winds in the Greenland and Norwegian seas under

NAO– conditions (Fig. 12B), driven by an anticyclonic cell centered on Greenland (Wanner et al., 2001).

Linear trends presented in Section 3 showed a significant increase of Hs_{90} (up to 0.02 m yr^{-1}) and a counterclockwise rotation of Mwd winter-means (up to $-0.1^\circ \text{ yr}^{-1}$) at northern latitudes, contrasting with a fairly constant trend for Hs_{90} and a clockwise rotation of Mwd winter-means (up to $+0.15^\circ \text{ yr}^{-1}$) at southern latitudes. Long-term trends for winter-means of Tp are less significant, with still a slight increase in the north-eastern part of the study area (up to $+0.01 \text{ s yr}^{-1}$). The contour maps of the spatial distribution of long-term trends for Hs_{90} , Mwd and Tp (Fig. 9) display striking similarities with the contour maps of correlations between the WNAO index and the respective wave parameters (Fig. 10). Based on these similarities, a regression analysis was performed on the WNAO index between 1953 and 2009 and resulted in a positive trend of $5.2\% \text{ yr}^{-1}$. This trend is supported by the large values of the WNAO index that occurred in the late 1980s that were shown by Hurrell (1995) to be the largest values ever recorded from 1864. Consequently, this increase in the WNAO index can directly explain the positive long-term trends for Hs_{90} and Tp at northern latitudes and the clockwise rotation of Mwd at southern latitudes.

This study has confirmed that, over the last six decades, the wave climate over the NEA has undergone considerable changes, not only with regard to wave height but also to direction and period. The temporal scales of these variations ranged from seasonal to pluri-decadal scales (>50 years) and were found to be highly spatial dependent. Indeed, over the study area, opposite trends were observed for each wave parameters considered, so one must be extremely cautious when extrapolating the conclusions obtained from one site to another. For example, the increase in coastal erosion observed in western Europe in the last fifty years (Eurosion, 2003) could be related to the roughening of the wave

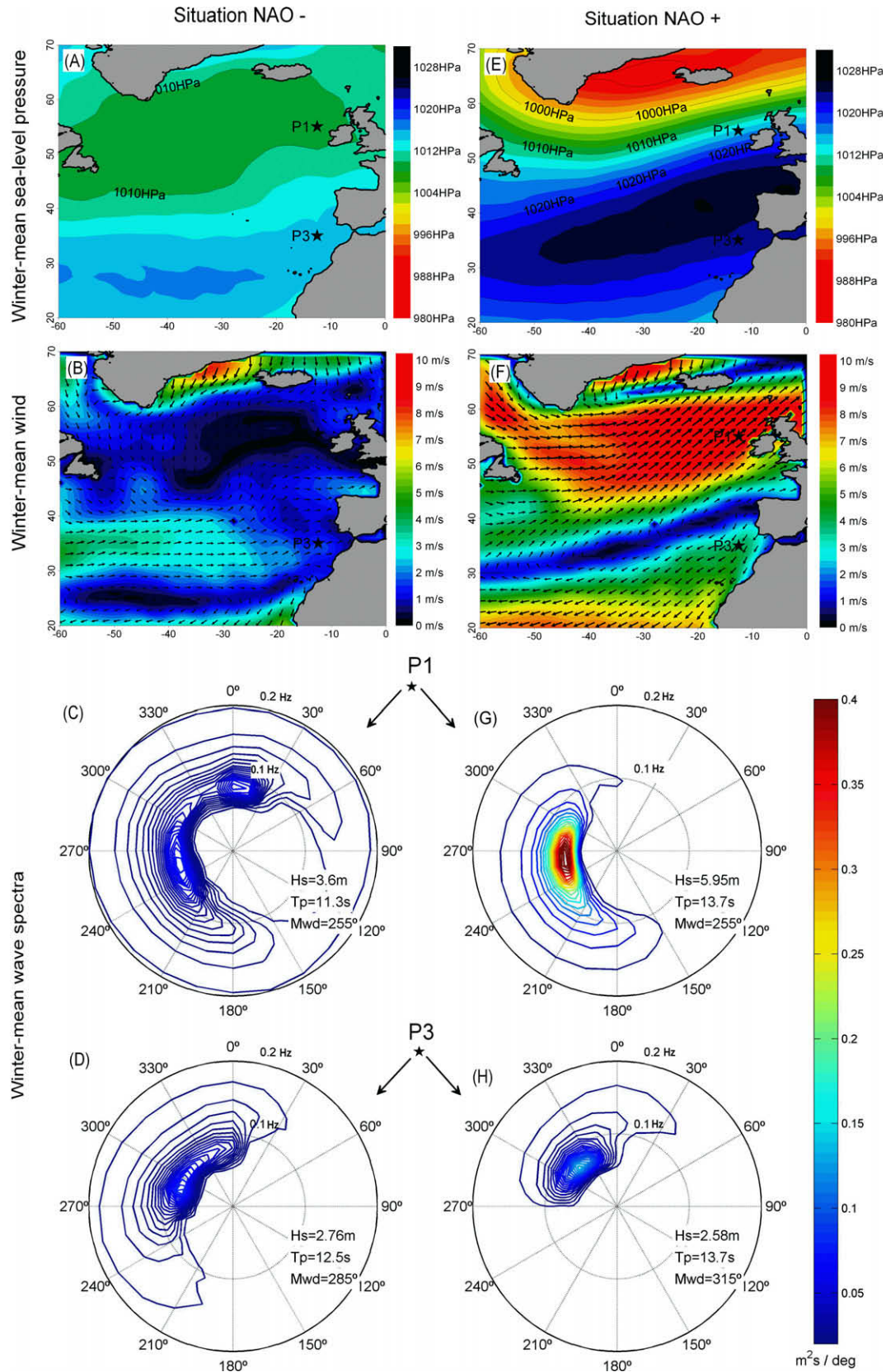


Fig. 12. Winter-mean SLP, winter-mean wind velocity over the North Atlantic Ocean and winter-mean wave spectra at P1 (12.5°W; 55.0°N) and P3 (12.5°W; 35.0°N) for the case “NAO-” in winter 1969 (A–D, respectively) and for the case “NAO+” in winter 1989 (E–H, respectively).

climate observed in northern Europe (+1.2 m for Hs_{90}) and not only to long-term sea-level rise (Bruun, 1962) and decrease in sediment supply from rivers (Paskoff, 2004). However coastal erosion

observed at southern latitudes cannot be attributed to the same mechanism as wave height trend was almost null. Instead, it might be connected to the detected clockwise rotation of winter-mean

Mwd (up to 8°), which can increase longshore drift and disturb the coastal sediment budget (Andrade et al., 2007).

The results obtained in the scope of this work put in evidence the strong link between the ocean and atmospheric climate dynamics, since inter-annual and long-term variabilities of Hs, Tp and Mwd were found to be significantly related to the WNAO index. Several hypotheses were proposed to explain the origin of NAO, such as changes in the rate and location of tropical heating (Hoerling et al., 2004) or interactions with the lower stratosphere (Cohen et al., 2002), but NAO is still a matter of debate in the scientific community and further research will be necessary to advance our understanding on this still weakly predictable phenomenon (Hurrell and Deser, 2009). Alternatively, the availability of the NAO index for the last 150 years and even reconstructions of this index since the 16th century by means of climate models (Luterbacher et al., 2002) would allow extending backward in time the investigation and understanding of past wave climate.

Acknowledgments

The first author was awarded a research fellowship funded by the Portuguese Science and Technology Foundation (FCT) in the framework of the project *BAYBEACH – Evolution and Management of Embayed Beaches in Contrasting Environments* (ref: PTDC/CTE-GEX/66893/2006) and was hosted by the Faculty of Sciences of the University of Lisbon and the National Laboratory of Civil Engineering. This work is also a contribution to the European project *MICORE – Morphological Impacts and Coastal Risks induced by Extreme storm events* (Grant agreement no.: 202798) and the FCT project *G-Cast – Application of GRID-computing in a coastal morphodynamics now-cast-forecast system* (ref: GRID/GRI/81733/2006).

This research would not have been possible without the availability of the WAVEWATCH III™ model and the NCEP Reanalysis data provided by the NOAA/OAR/ESRL PSD.

The quality of the model results owes much to the very kind help of Fabrice Ardhuin (Service Hydrographique et Océanographique de la Marine, France). In-situ data necessary for the model validation were provided by the Puertos del Estado in Spain, the Sistema Nacional de Informação dos Recursos do Litoral (SNIRLIT) in Portugal and the British Oceanographic Data Center for the Ocean Weather Station “Juliett”.

The authors are grateful to André Fortunato, who carried out a final check of the paper. Finally, the recommendations of three anonymous reviewers were greatly appreciated and permitted to improve the manuscript significantly.

References

- Andrade, C., Pires, H.O., Taborda, R., Freitas, M.C., 2007. Projecting future changes in wave climate and coastal response in Portugal by the end of the 21st century. *Journal of Coastal Research* 51, 253–257.
- Ardhuin, F., Martin-Lauzer, F.R., Chapron, B., Craneguy, P., Girard-Ardhuin, F., Elfouhaily, T., 2004. Wave-induced drift at the ocean surface. *Comptes Rendus Geoscience* 336, 1121–1130.
- Ardhuin, F., Chapron, B., Collard, F., 2009a. Strong decay of steep swells observed across oceans. *Geophysical Research Letters* 36. doi:10.1029/2008GL037030.
- Ardhuin, F., Marié, L., Rasclé, R., Forget, P., Roland, A., 2009b. Observation and estimation of Lagrangian, Stokes and Eulerian currents induced by wind and waves at the sea surface. *Journal of Physical Oceanography*. doi:10.1175/2009JP04169.1.
- Bacon, S., Carter, D.J.T., 1991. Wave climate changes in the north Atlantic and North Sea. *International Journal of Climatology* 11, 545–558.
- Bacon, S., Carter, D.J.T., 1993. A connection between mean wave height and atmospheric pressure gradient in the North Atlantic. *International Journal of Climatology* 13, 423–436.
- Banner, M.L., Babanin, A.V., Young, I.R., 2000. Breaking probability for dominant waves on the sea surface. *Journal of Physical Oceanography* 30, 3145–3160.
- Bauer, E., 2001. Interannual changes of the ocean wave variability in the North Atlantic and in the North Sea. *Climate Research* 18, 63–69.
- Bidlot, J., Janssen, P., Abdalla, S., 2007a. A revised formulation of ocean wave dissipation and its model impact. Tech. Rep. Memorandum 509, ECMWF, Reading, UK.
- Bidlot, J.-R., Li, J.-G., Wittmann, P., Fauchon, M., Chen, H., Lefèvre, J., Bruns, T., Greenslade, D., Ardhuin, F., Kohno, N., Park, S., Gomez, M., 2007b. Inter-comparison of operational previous termwavenext term forecasting systems. In: *Proceedings of the 10th Int. Workshop of Previous TermWavenext Term Hindcasting and Forecasting*, Hawaii, 22pp.
- Black, K.P., Oldman, J.W., 1999. Wave mechanisms responsible for grain sorting and non-uniform ripple distribution across two moderate-energy, sandy continental shelves. *Marine Geology* 162, 121–132.
- Bruun, P., 1962. Sea level rise as a cause of shore erosion. *Journal of Waterways, Ports and Harbours Division* 88 (1–3), 117–130.
- Carter, R.W.G., 1988. *Coastal Environments. An Introduction to the Physical, Ecological and Cultural Systems of the Coastlines*. Academic Press, New York, 617 p.
- Challenor, P., Woolf, D., Gommenginger, C., Srokosz, M., Cotton, D., Carter, D., Sykes, N., 2006. Satellite altimetry: a revolution in understanding the wave climate in 15 years of Progress in Radar Altimetry Symposium, Venice, 13–18 March 2008.
- Cohen, J., Salstein, D., Saito, K., 2002. A dynamical framework to understand and predict the major Northern Hemisphere mode. *Geophysical Research Letter* 29, 1412.
- Dupuis, H., Michel, D., Sottolichio, A., 2006. Wave climate evolution in the Bay of Biscay over two decades. *Journal of Marine Systems* 63, 105–114.
- EuroSION, 2003. *Trends of Coastal Erosion in Europe*. EuroSION Project, Final Version Report. Available at: <http://www-euroSION.org>.
- Filipot, J.-F., Ardhuin, F., Babanin, A., 2008. Paramétrage du déferlement des vagues dans les modèles spectraux: approches semi-empirique et physique. In: *Proceedings of the 10th Journées Génie Côtier-Génie Civil*, Sophia Antipolis, France, pp. 335–344.
- Hoerling, J.W., Hurrell, T., Xu, G.T., Bates, Phillips, A.S., 2004. Twentieth century North Atlantic climate change. Part II. Understanding the effect of Indian Ocean warming. *Climate Dynamic* 23, 391–405.
- Hurrell, J.W., 1995. Decadal trends in the North Atlantic Oscillation: regional temperatures and precipitations. *Science* 269, 676–679.
- Hurrell, J.W., Dickson, R.R., 2004. Climate variability over the North Atlantic. In: Stenseth, N.C., Ottersen, G., Hurrell, J.W., Belgrano, A. (Eds.), *Marine Ecosystems and Climate Variation – The North Atlantic*. Oxford University Press, 2004.
- Hurrell, J.W., Deser, C., 2009. North Atlantic climate variability: the role of the North Atlantic Oscillation. *Journal of Marine Systems* 78 (1), 28–41.
- IPCC, 2007. *Climate change 2007: impacts, adaptation and vulnerability*, Working Group I Report, The Physical Science Basis, Chapter 10, Global Climate projection, World Meteorological Organization, Genève, 2007, pp. 812–822.
- Janssen, P.A.E.M., 1991. Quasi-linear theory of wind wave generation applied to wave forecasting. *Journal of Physical Oceanography* 21, 1631–1642.
- Kalnay, E., Kanamitsu, M., Kistler, R., Collins, W., Deaven, D., Gandin, L., Iredell, M., Saha, S., White, G., Woollen, J., Zhu, Y., Chelliah, M., Ebisuzaki, W., Higgins, W., Janowiak, J., Mo, K.C., Ropelewski, C., Wang, J., Leetmaa, A., Reynolds, R., Roy Jenne, R., Joseph, D., 1996. The NCEP/NCAR 40-year reanalysis project. *Bulletin of the American Meteorological Society* 77, 437.
- Kushnir, Y., Cardone, V.J., Greenwood, J.G., Cane, M.A., 1997. The recent increase in North Atlantic wave heights. *Journal of Climate* 10, 2107–2113.
- Longuet-Higgins, M.S., Stewart, R.W., 1964. Radiation stresses in water waves; a physical discussion, with applications. *Deep-Sea Research* 11, 529–562.
- Luterbacher, J., Xoplaki, E., Dietrich, D., Jones, P.D., Davies, T.D., Portis, D., Gonzalez-Rouco, J.F., von Storch, H., Gyalistras, D., Casty, C., Wanner, H., 2002. Extending North Atlantic Oscillation reconstructions back to AD 1500. *Atmospheric Science Letters* 2, 114–124.
- Paskoff, R., 2004. Potential implications of sea-level rise for France. *Journal of Coastal Research* 20 (2), 424–434.
- Rasclé, N., Ardhuin, F., Queffeuilou, P., Croizé-Fillon, D., 2008. A global wave parameter database for geophysical applications. Part 1: Wave-current-turbulence interaction parameters for the open ocean based on traditional parameterizations. *Ocean Modelling* 25 (3–4), 154–171.
- Smith, W.H.F., Sandwell, D.T., 1997. Global seafloor topography from satellite altimetry and ship depth soundings. *Science* 277, 1957–1962.
- The WASA Group, 1998. Changing waves and storm in the Northeast Atlantic? *Bulletin of the American Meteorological Society* 79, 741–760.
- Tolman, H.L., 2002. Treatment of unresolved islands and ice in wind wave models. *Ocean Modelling* 5, 219–231.
- Tolman, H. L., 2009. User manual and system documentation of WAVEWATCH III version 3.14. NOAA/NWS/NCEP/MMAB Technical Note 276, 194 p.
- Walden, H., Hogben, N., Burkhart, M.D., Dorrestein, R., Warnsink, W.H., Yamanouchi, Y., 1970. Long Term Variability. In: 4th International Ship Structures Congress, Tokyo, Group of Committee 1, pp. 49–59.
- WAMDI Group, 1988. The WAM model – a third generation ocean wave prediction model. *Journal of Physical Oceanography* 18, 1775–1809.
- Wang, X., Swail, V., 2001. Trends of atlantic wave extremes as simulated in a 40-yr wave hindcast using kinematically reanalyzed wind fields. *Journal of Climate* 15, 1020–1035.
- Wanner, H., Brönnimann, S., Casty, C., Gyalistras, D., Luterbacher, J., Schmutz, C., Stephenson, D.B., Xoplaki, E., 2001. North Atlantic Oscillation – Concepts and Studies. *Surveys in Geophysics* 22, 321–382.
- Woolf, D.K., Cotton, P.D., Challenor, P.G., 2002. Variability and predictability of the North Atlantic wave climate. *Journal of Geophysical Research* 107 (C10), 9–23.